J Mater Sci: Mater Electron

# The application of biomass-based carbon materials in flexible all-solid supercapacitors

Xiao Zhang[1], Mei Zhao[1], Zejian Chen[1,2], Tong Yan[1,2], Jiangli Li[1], Yanqing Ma[1,*], and Lei Ma[1,*]

[1] Tianjin International Center for Nanoparticles and Nanosystems, Tianjin University, Tianjin 300072, People's Republic of China
[2] School of Chemistry and Chemical Engineering, Shihezi University, Shihezi 832003, People's Republic of China

**Received:** 3 January 2022
**Accepted:** 18 May 2022



## ABSTRACT

Four different kinds of carbon materials were synthesized successfully from saussurea involucrata, cotton stalk and cellulose by two activation methods (KOH-chemical activation method and mixed molten-salt synthesis). Carbon structures, electrochemical and flexible properties are studied. The saussurea involucrata-based flexible symmetric all-solid states supercapacitor exhibited high electrochemical performances, including high specific capacitance (129 F $g^{-1}$ at 2 mV $s^{-1}$) and excellent cycle stability ($\sim$ 85% capacitance retention even after 10,000 cycles). More importantly, it also displays excellent bending endurance, the specific capacitance is almost unchanged after 100 bends. This study shows promising materials in symmetric all-solid state supercapacitor applications.

## 1 Introduction

In recent decades, the relationship between energy and environment has drown more and more attention [1–4]. The development of energy storage devices became more importantly. Among various energy storage devices, supercapacitors have many special performances, such as short charge/discharge rate, long cycling reliability and safety. Meanwhile, with the development of flexible wearable devices, flexible supercapacitors have become a significant and inevitable trend [5–7].

As the electrode active material of supercapacitors, biomass-based activated carbon materials have many advantages, especially in environmental protection, easily available and low cost [5, 8–10]. Many kinds of biomass-based activated carbon materials have been successfully used in supercapacitor electrodes, such as banana peel [11], soybean milk [12], chitosan [13], basil seed,[14] areca palm leaves,[15] wheat straw,[16] tassel tree flowers,[17] wax gourd[18] and cotton leaf [19]. As a king of waste byproduct, cotton stalk often has been dumped or burned in the field, which resulting in ash and hazardous gas emissions [20, 21]. Cellulose is a widely present and renewable

Xiao Zhang and Mei Zhao have contributed equally to this paper.

Address correspondence to E-mail: mayanqing@tju.edu.cn; lei.ma@tju.edu.cn

https://doi.org/10.1007/s10854-022-08449-6
Published online: 08 June 2022

resource in nature. It possesses high carbon content and widely used as precursors in supercapacitors [22, 23]. More importantly, our group also successfully obtained porous carbon materials with the cotton stalks [20], saussurea involucrate [24] and cellulose [22]. They all exhibited excellent performances in traditional supercapacitors. However, the electrochemical properties in flexible all-solid states supercapacitors (ASSC) with these carbon materials are still unknown. Based on this, we intend to study whether they have good performances in ASSC. Meanwhile, as far as we know, there is few systematic reports concern about the different materials in flexible all-solid states supercapacitors. Therefore, using efficient and simple ways to find a good carbon structure in ASSC would be critical for flexible all-solid states supercapacitors.

In this work, the mixed salts activation strategy and KOH activation method were employed as two activation agents to prepare porous carbon, three common precursors (saussurea involucrata, cotton stalk and cellulose) were used as precursors. By studying these carbon materials, the proper carbon materials with high electrochemical performances as well as excellent mechanical properties are obtained. This study will give guidance when selecting the suitable carbon materials for symmetric all-solid supercapacitor.

## 2 Experiment

### 2.1 Materials preparation

Biomass precursors (cotton stalk, saussurea involirata and cellulose) were transferred into a tubular furnace for carbonation under the protection of nitrogen, then the biomass powder was heated to 400 °C at a heating rate of 5 °C $min^{-1}$ and maintained for 1 h, then the sample was cool down to room temperature at cooling rate of 5 °C $min^{-1}$ to obtain carbon precursor.

Two strategies were used to prepare of electrode material.

In the first activated process, three product were mixed with KOH (the mass ratio is 1:4) respectively and transferred in a tubular furnace to pyrolysis. Then heated to 800 °C at a rate of 5 °C $min^{-1}$ and maintained at this temperature for 2 h. The all processes are under the protection of Ar. After obtaining the porous carbon, put it into a beaker with 10% HCl and stir for 24 h. The samples were washed with deionized water and then the electrode material can be obtained after totally drying at 50 °C for 12 h. The related samples were marked as SAK, CSAK.

As for second activated process, three carbon products were mixed with KOH and NaCl (the pre-carbonized sample: KOH: NaCl = 1:4:1). The mixtures were activated at 800 °C for 2 h. The all processes are under the protection of Ar. After obtaining the porous carbon, put it into a beaker with 10% HCl and stir for 24 h. The samples were washed with deionized water and then the electrode material can be obtained after totally drying at 50 °C for 12 h. The related samples were marked as CSAN and CAN.

### 2.2 Fabrication of the electrode

The carbon material, acetylene black and polytetrafluoroethylene (PTFE) were mixed at a mass ratio of 8:1:1. The mixture was rolled into a round plate with a diameter of 8 mm. The loading mass of each active materials on each electrode was $\sim$ 1.5 mg.

### 2.3 Electrochemical measurement

The all-solid-state flexible supercapacitor was assembled from two identical electrodes, wherein PVA/LiCl gel was used as the electrolyte. For preparing the PVA/ LiCl gel, 10 g PVA and 20 g LiCl were mixed with 100 mL deionized water. Then, the obtained mixture was heated to 80 °C with vigorous stirring until it became clear. Then, two electrodes were overlayed the carbon cloth head-to-head for 20 min. As a result, after packaging, the all-solid-state symmetric SC device was obtained.

Electrochemical performance measurements were carried out in a two-electrode system by a cyclic voltammetry (CV), electrochemical impedance spectroscopy (EIS) and charge–discharge performance of supercapacitors was studied on a CHI 760E electrochemical workstation. CV test of the two-electrode cell were investigated between 0.8 and 0 V. EIS measurements were performed by an AC voltage with 5 mV amplitude in a frequency range from 0.01 Hz to 100 kHz at the open circuit potential. The tests of cycle life were performed on a land cell taster (Land, CT-2001A).

According to the charge/discharge curves, the specific capacitance of electrodes can be calculated based on the following equation:

$$C_m = \frac{I_d \times \Delta t}{\Delta V \times m}$$

where $C_m$ (F $g^{-1}$) is specific capacitance, $I_d$ (mA) is the discharge current, $\Delta t$ (s) is the discharge time and $\Delta V$ (V) is the discharge voltage range, $m$ (mg) is the mass loading of active materials based on both electrodes.

Energy density $E$ (Wh $kg^{-1}$) and power density $P$ (W $kg^{-1}$) were calculated according to the following equations:

$$E = \frac{1}{2} C_m \times \Delta V^2 \times \frac{1}{3.6}$$

$$P = \frac{E}{\Delta t} \times 3600$$

where the $C_m$ (F $g^{-1}$) is specific capacitance based on mass loading of active materials in both electrodes, $\Delta V$(V) is the discharge voltage range that is exclusive of the IR drop, $\Delta t$(s) is the discharge time.

## 3 Results and discussion

Scheme 1 shows the main process of preparing supercapacitor. The first step is to cut the carbon cloth with area of 1 cm × 3 cm. And then attach the prepared electrode to the end of carbon cloth. Applying the PVA/LiCl on it. Finally covered electrolyte and carbon cloth with another electrode to obtain a ASSC.

Figure 1a–d show the typical SEM images of four samples after activation. It can be seen clearly that all samples exhibit various disordered porous channel structure. Compared with Fig. 1a, b, SAK exhibits porous square structure. The grooves in these squares are activated by KOH activation. CSAK not only shows open and porous structure, but also forms a flute-like structure with KOH activation. The pore size of CSAK is about 3 μm. Meanwhile, CSAN and CAN show thinner and shaggy morphology with a molten-salt synthesis in Fig. 1c, d. CSAN has bigger holes and thinner carbon wall than CAN. In general, compared with CSAN and CAN, materials activated by KOH (SAK and CSAK) have more macropores and thicker carbon wall. This stronger 3D porous carbon skeleton made them decrease mechanical damage effectively during the practical application. Thus, they exhibit excellent mechanical properties, as can be confirmed in Fig. 6.

Lattice stripes of SAK can be clearly observed in Fig. 2a because of the instability alkyl chains and some linkages between monomer units and the methoxy substituents of the aromatic rings, which are generally accompanied by the release of water or gas [25]. Figure 2b presents an unevenly macroporous structure. Macropores are formed by the structure of the cotton stalk itself. Figure 2c exhibits the loose carbon structures of CSAN formed by the NaCl at high temperature. NaCl spread into the tube bundles, which are favorite for the mixing of the molten salt and precursor and finally leads to the formation of porous carbon sheets under air atmosphere [26, 27]. Because CAN is microcrystalline cellulose. The NaCl is easier to insert into the sample, the carbon layer is thinner than other materials in Fig. 2d.

The intrinsic properties of the samples were analyzed by XRD and Raman spectra. Figure 3a shows the XRD patterns of four activated carbon samples, a typical diffraction peak at approximately 22° and 43° demonstrate the diffractions peak of (002) and (100) planes of graphitic carbon and disordered carbon [28–30]. The broad peaks of carbon are due to the

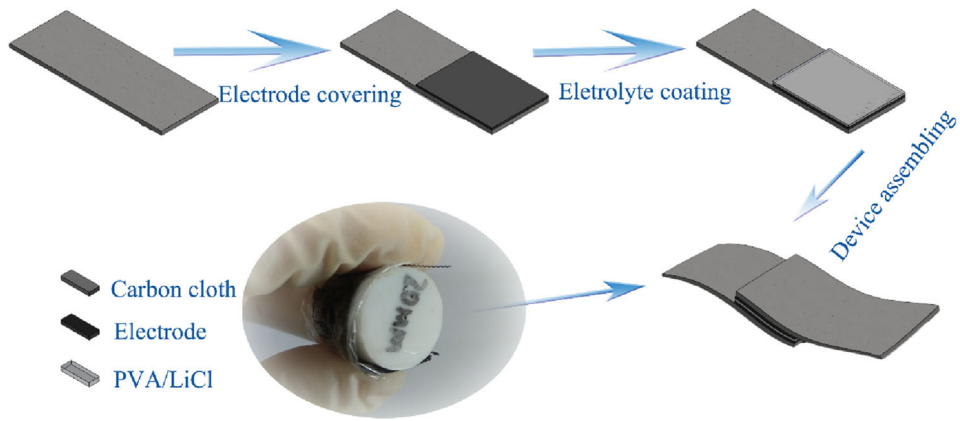


**Scheme 1** Schematic of the flexible all-solid states supercapacitor

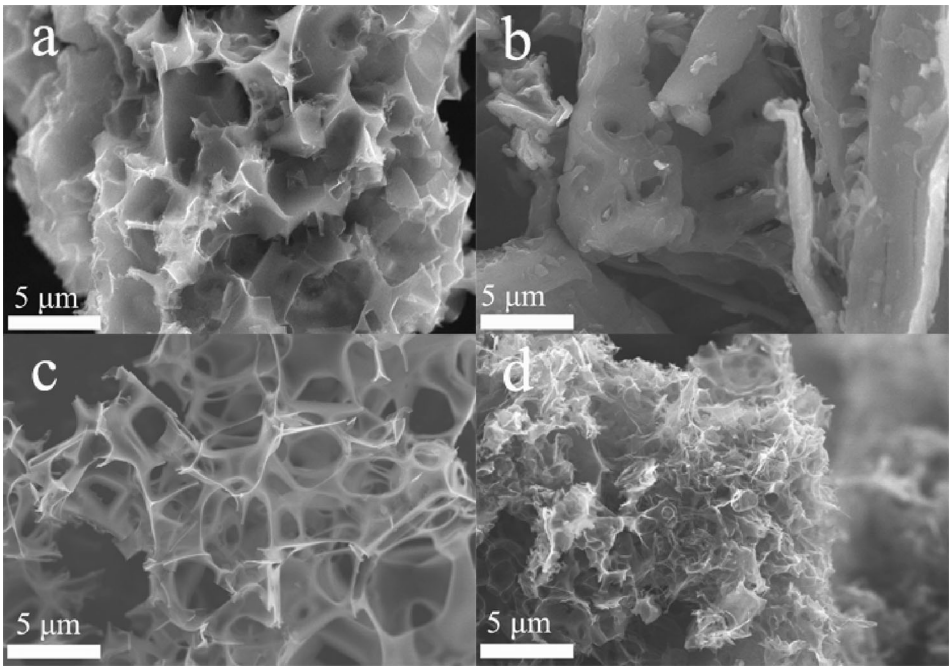


**Fig. 1** The representative SEM images of all samples at the magnifications: **a** SAK; **b** CSAK; **c** CSAN; **d** CAN

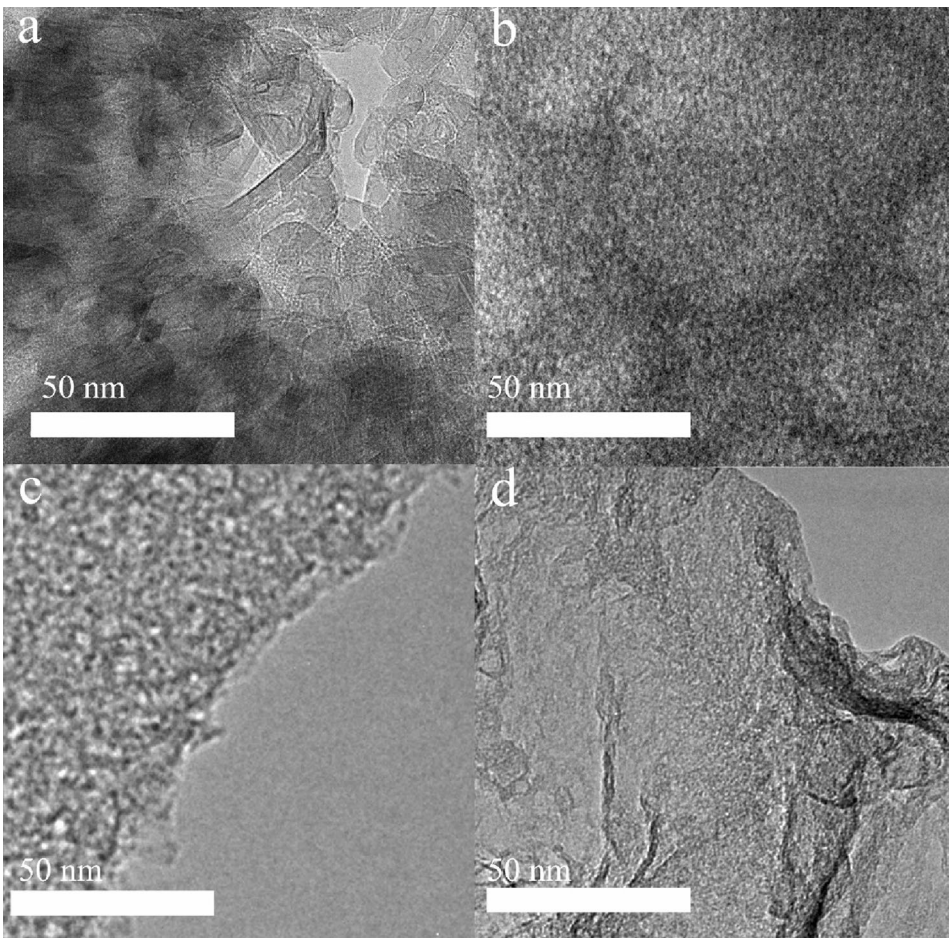


**Fig. 2** The representative TEM images of all samples at the magnifications: **a** SAK; **b** CSAK; **c** CSAN; **d** CAN

abundant micropores, confirming the amorphous carbon structure [31–33]. As for SAK and CSAK, the peak of (002) plane show an obviously broaden and disappeared trend compared with CAN and CSAN. The increase of diffraction intensity at low scattering angles ($2\theta < 10°$) indicates the increased amount of micropores [34]. Raman spectra further explores the physicochemical properties of the synthesized carbon materials in Fig. 3b. All samples have two typical carbon characteristic diffraction peaks appeared in 1360 $cm^{-1}$ (D peak) and 1586 $cm^{-1}$ (G peak). D peak with a double-resonance represents the degree of disordered structure or structural defects. G peak corresponding to graphite in-plane vibrations represents an ordered carbon [35–38]. The calculated relative intensity ratio values ($I_D/I_G$) for all samples is 0.89 (SAK), 0.91 (CSAK), 1.01 (CSAN) and 1.03 (CAN). The larger $I_D/I_G$ value is, the more defects and lower graphitization degree are found in carbon crystal [39, 40]. It indicates that SAK and CSAK have higher graphitization degree and better conductivity [22, 41–43]. This is because KOH can react with carbon to make more graphitized carbon [44, 45]. It also shows CSAN and CAN have more disordered structure and have more defects.

Furthermore, the porous properties of samples were examined with $N_2$ adsorption/desorption isotherms, four samples were characterized at 77 K as shown in Fig. 3c. And the corresponding pore size distributions of the samples calculated using the nonlinear density functional theory (DFT). The $N_2$ adsorption amount of SAK and CSAK is higher than CSAN and CAN, which is because the KOH activator can effectively generate micropores and middle holes in various structural carbons. The surface area was calculated by the standard BET method show in Table 1. This confirms that carbon activated by KOH can efficiently increase the specific surface area. As can be seen from Fig. 3d, SAK and CSAK have more obvious peaks at 0.5–1.5 nm, which is suitable for the diffusion of electrolyte ions [46]. The properties of the samples are summarized in Table 1. The BET surface area is calculated to be 2073 $m^2\ g^{-1}$, 1964 $m^2\ g^{-1}$, 826

**Table 1** Textural characteristic properties of the porous carbon

| Sample | $S_{BET}$ ($m^2\ g^{-1}$) | $V_{total}$ ($cm^3\ g^{-1}$) |
|---|---|---|
| CSAN | 826 | 0.46 |
| CAN | 822 | 0.50 |
| SAK | 2073 | 0.89 |
| CSAK | 1964 | 1.03 |

Obtained by DFT method

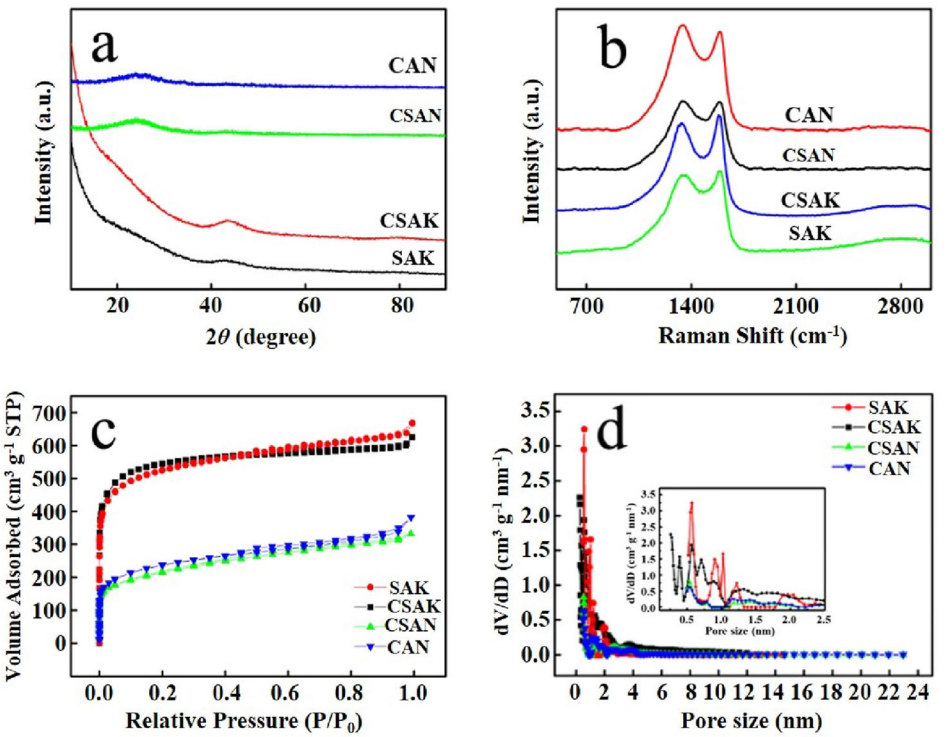


**Fig. 3** **a** XRD patterns; **b** Raman spectra; **c** Nitrogen adsorption–desorption isotherms; **d** Pore size distribution, calculated from the adsorption isotherms using DFT method. The inset shows magnified section of pore diameter ranging from 0 nm to 2.5 nm

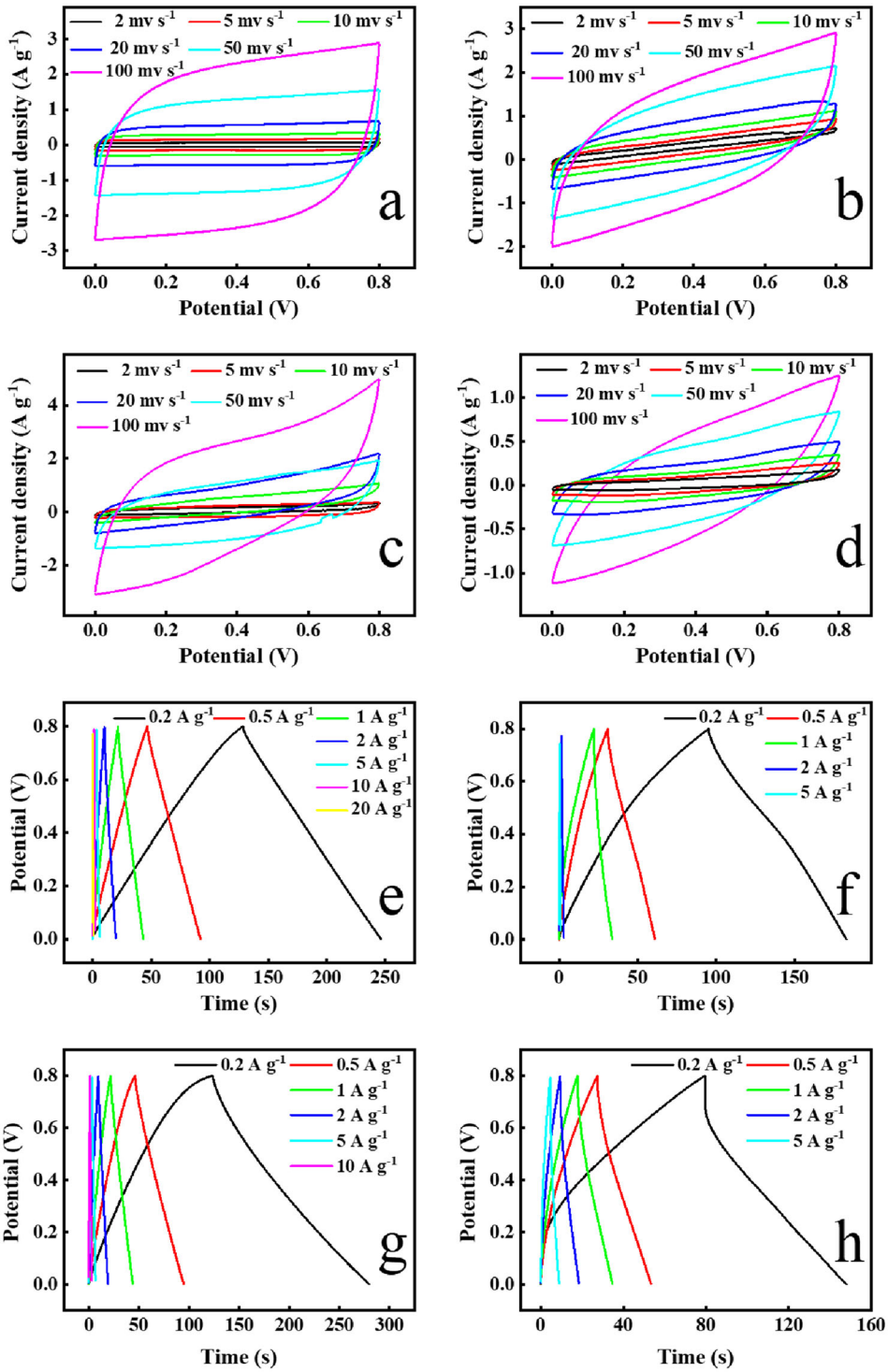


**Fig. 4** CV curves of four electrodes at various scan rates ranging from 2 to 100 mV $s^{-1}$ in PVA/LiCl electrolyte: **a** SAK; **b** CSAK; **c** CSAN; **d** CAN. The galvanostatic charge–discharge curves of **e** SAK; **f** CSAK; **g** CSAN; **h** CAN

$m^2$ $g^{-1}$ and 822 $m^2$ $g^{-1}$ for SAK, CSAK, CSAN and CAN, respectively. The SAK has the highest surface area than other samples, which made it store more charges. These results suggested that KOH activation greatly enhanced the development of pores during activation. The active ions from KOH will intercalate with the carbon matrix, widening the space between carbon layers and enhances the total pore volume.

All carbon materials were made into electrodes and assembled into symmetric ASSCs. The

electrochemical performance was measured using cyclic voltammetry (CV) and galvanostatic cycling techniques. Figure 4a–d show the CV curves at different scan rates from 2 to 100 mV $s^{-1}$. All CV curves are approximately rectangular, and no other redox peaks exist. These mean typical characteristics of double layer capacitance. Among these CV curves, SAK exhibits better rectangular shape than other materials. When the scan rates increasing, SAK shows no obvious deformation with the increasing scan rate. It is indicating more ideal electrical double-layer capacitive behavior than others, which results from the higher porosity and narrower hole distribution of SAK. At 2 mV $s^{-1}$, the specific capacitances of SAK, CSAK, CSAN and CAN are 129 F $g^{-1}$, 133 F $g^{-1}$, 176 F $g^{-1}$ and 90 F $g^{-1}$. At 100 mV $s^{-1}$, the specific capacitances of SAK, CSAK, CSAN and CAN are 98 F $g^{-1}$, 57 F $g^{-1}$, 88 F $g^{-1}$ and 26 F $g^{-1}$. Meanwhile, the specific capacitance of SAK can reach 129 F $g^{-1}$ at 2 mV $s^{-1}$, which is higher than other symmetric ASSC [28, 47–50], even other supercapacitors of aqueous electrolytes [51]. Figure 4e–h present the galvanostatic charge–discharge (GCD) curves at various current densities. There is no obvious voltage drop in these materials except CAN, indicating that the material has good conductivity and small and negligible internal resistance. As the current density increases, the charging time decreases and the shape of the curve remains the same. The specific capacitance of SAK, CSAK, CSAN and CAN electrodes at 0.2 A $g^{-1}$ are 118 F $g^{-1}$, 88 F $g^{-1}$, 150 F $g^{-1}$ and 68 F $g^{-1}$, respectively. Electrode derived from SAK can work at larger current density (20 A $g^{-1}$). It indicates that SAK has better capacitive behavior than others.

Figure 5 shows the cyclic charge–discharge test of all-solid states supercapacitor at 10 A $g^{-1}$. The specific capacitance increases initial and then decreases. In the initial cycles, the capacitive retention increases, which is related to electrode activation. Electrolyte ions permeate the material and improve the utilization rate of the material. After 6000 cycles, the specific capacitance of CSAK, CSAN and CAN remains 85%, 80% and 75%. While the specific capacitance of SAK can remain 85% even after 10,000 cycles of charge and discharge. It is proved that the all-solid states symmetric supercapacitor based on these materials have a long cycling life.

In order to further study the charge transfer resistance within these materials in PVA/LiCl electrolyte,

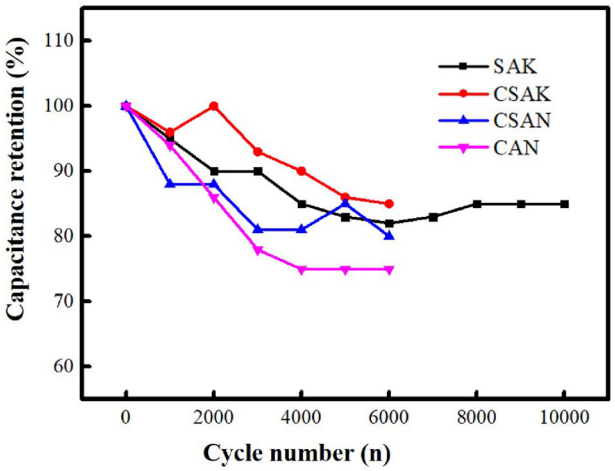


**Fig. 5** Cycle stability performance of the SAK, CSAK, CSAN and CAN at 10 A $g^{-1}$ in PVA/LiCl

the Nyquist plot was collected by electrochemical impedance spectroscopy (EIS) in Fig. 6c. The $R_e$ is resistance and $R_{ct}$ is charge transfer resistance. The frequency range is from 0.01 Hz to 100 kHz. The open circuit potential is 5 mV. The simulation of Nyquist plot shows there is apparent semicircle in the high-frequency range which is caused by the electric double-layer capacitance. The $R_e$ and $R_{ct}$ of SAK is 6.0 Ω and 0.8 Ω. The $R_e$ and $R_{ct}$ of CSAK is 3.0 Ω and 1.4 Ω. This phenomenon shows that the resistance of SAK is bigger than that of CSAK, but charge transfer resistance of SAK is smaller than CSAK's. It means that the SAK is more suitable for working at high current density, this corresponds to the result in Fig. 4e. The energy density and power density of flexible ASSC were shown in Ragone plot in Fig. 6f. The highest energy density of SAK and CSAK are 10.5 W h $kg^{-1}$ and 7.8 W h $kg^{-1}$ when the power density of two samples are both 320 W $kg^{-1}$.

In order to verify the flexibility of ASSC and its application in wearable electronics. We tested the electrical properties under different bending radius in Fig. 6. Figure 6a shows CV cures of SAK with 0–20 mm bending radius at 20 mV $s^{-1}$. The CV cures are exhibited a rectangular shape at different bending radius. After calculation, the fluctuation of specific capacitance is 84–92 F $g^{-1}$. Figure 6d shows the CV cure of SAK under 10–100 times bending. After bending 100 times, SAK still has better rectangular shape. The specific capacitance change is no more than 10% after bending 100 times. The curve shows very small relative changes compared to the previous

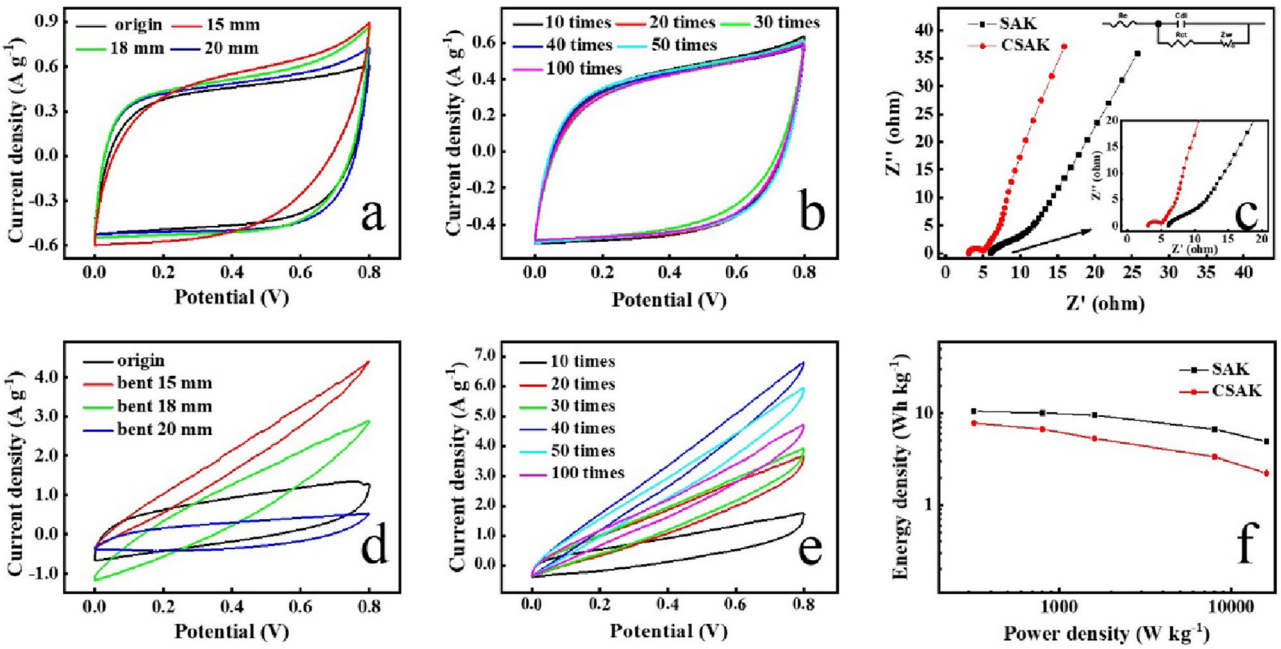


**Fig. 6** **a**, **d** CV curves of SAK and CSAK electrodes in various bending radius from 0 to 20 mm at 20 mV $s^{-1}$; **b**, **e** CV curves of SAK and CSAK electrodes in various bending times from 10 to 100 at 20 mV $s^{-1}$; **c** Nyquist plots of SAK and CSAK in PVA/LiCl (The inset shows the magnified view of the high-frequency region and the electrical equivalent circuit used for fitting impedance spectra); **f** Ragone plots of SAK and CSAK

one. After calculation, the fluctuation of specific capacitance in different bending times is 77–82 F $g^{-1}$ at scan rate of 20 mV $s^{-1}$, which shows good bending stability. These electrochemical performance analyses suggest that SAK is promising electrode material for fabricating ASSC due to high specific capacitance and good flexibility. As for other materials, the flexible performances are not as optimistic as SAK. As shown in Fig. S5, the CV cures are not presentative rectangular after bending. It means other carbon structure is not suitable for flexible ASSC. SAK not only has long and big clod flute porous carbon to obtain excellent electrochemical performances, but also has a 3D carbon skeleton to endure some mechanical damage. It indicates SAK has great potential in wearable electronics.

## 4 Conclusion

In summary, different carbon materials have been obtained with three materials and two methods. Saussurea involucrata activated by KOH has large specific area (2073 $m^2$ $g^{-1}$), reasonable pore distribution and 3D carbon skeleton. When assembled flexible supercapacitors with PVA/LiCl, it exhibits higher specific capacitance, excellent cycle stability and flexibility. After 10,000 cycles, the capacitance can still retain 85%. The as-fabricated ASSC well retained its electrochemical performance even under harsh conditions. This result provides references for the preparation of electrode material in flexible supercapacitors.

## Acknowledgements

This work was financially supported by the National Natural Science Foundation of China (No. 11774255) and the National Key R&D Program of China (No. 2020YFC2004602).

## Author contributions

All authors contributed to the study conception and design. Material preparation, data collection and analysis were performed by XZ, MZ, YM and LM. The first draft of the manuscript was written by XZ, MZ and YM. ZC, TY and JL do the test of SEM. All authors read and approved the final manuscript. The whole manuscript was instructed by YM and LM.

## Funding

Funding was provided by National Natural Science Foundation of China (11774255) and National Key R&D Program of China (973 Program) (2020YFC2004602).

## Data availability

The datasets generated during and analyzed during the current study are available from the corresponding author on reasonable request.

## Declarations

**Conflict of interest** The work described was original research that has not been published previously, and not under consideration for publication elsewhere, in whole or in part. The authors have no relevant financial interests to disclose.

**Supplementary Information:** The online version contains supplementary material available at https://doi.org/10.1007/s10854-022-08449-6.

## References

1. X. Zhang, F. Tian, X. Lan, Y. Liu, W. Yang, J. Zhang et al., Building P-doped $MoS_2$/g-$C_3N_4$ layered heterojunction with a dual-internal electric field for efficient photocatalytic sterilization. Chem. Eng. J. **429**, 132588 (2022)
2. S. Bao, Y. Wang, Z. Wei, W. Yang, Y. Yu, Highly efficient recovery of heavy rare earth elements by using an amino-functionalized magnetic graphene oxide with acid and base resistance. J. Hazard. Mater. **424**, 127370 (2022)
3. X. Zhang, W. Yang, M. Gao, H. Liu, K. Li, Y. Yu, Room-temperature solid phase surface engineering of BiOI sheets stacking g-$C_3N_4$ boosts photocatalytic reduction of Cr(VI). Green Energy Environ. **7**(1), 66–74 (2022)
4. X. Zhang, F. Tian, M. Gao, W. Yang, Y. Yu, L-Cysteine capped Mo2C/$Zn_{0.67}Cd_{0.33}S$ heterojunction with intimate covalent bonds enables efficient and stable H2-Releasing photocatalysis. Chem. Eng. J. **428**, 132628 (2022)
5. Y. Yang, A mini-review: emerging all-solid-state energy storage electrode materials for flexible devices. Nanoscale **12**(6), 3560–3573 (2020)
6. P. Zhang, F. Wang, S. Yang, G. Wang, M. Yu, X. Feng, Flexible in-plane micro-supercapacitors: progresses and challenges in fabrication and applications. Energy Stor. Mater. **28**, 160–187 (2020)
7. C.B. Guilherme, A.C. Rodrigues, A. Cuña, P.A. Claudia, B.M. Ribeiro, Process of converting human hair into hollow carbon filament for electrochemical capacitor. Matéria. 26 (2021).
8. J. Zhou, S. Yuan, C. Lu, M. Yang, Y. Song, Hierarchical porous carbon microtubes derived from corn silks for supercapacitors electrode materials. J. Electroanal. Chem. **878**, 114704 (2020)
9. J. Wang, X. Zhang, Z. Li, Y. Ma, L. Ma, Recent progress of biomass-derived carbon materials for supercapacitors. J. Power Sources. **451**, 227794 (2020)
10. X. Liang, R. Liu, X. Wu, Biomass waste derived functionalized hierarchical porous carbon with high gravimetric and volumetric capacitances for supercapacitors. Microporous Mesoporous Mater. **310**, 110659 (2021)
11. K. Chaitra, R.T. Vinny, P. Sivaraman, N. Reddy, C.Y. Hu, K. Venkatesh et al., KOH activated carbon derived from biomass-banana fibers as an efficient negative electrode in high performance asymmetric supercapacitor. J Energy Chem. **26**(1), 56–62 (2017)
12. D. Yu, Y. Ma, M. Chen, X. Dong, KOH activation of wax gourd-derived carbon materials with high porosity and heteroatom content for aqueous or all-solid-state supercapacitors. J. Colloid Interface Sci. **537**, 569–578 (2019)
13. K. Chen, S. Weng, J. Lu, J. Gu, G. Chen, O. Hu et al., Facile synthesis of chitosan derived heteroatoms-doped hierarchical porous carbon for supercapacitors. Microporous Mesoporous Mater. **320**, 111106 (2021)
14. H. Yang, J. Zhou, M. Wang, S. Wu, W. Yang, H. Wang, From basil seed to flexible supercapacitors: green synthesis of heteroatom-enriched porous carbon by self-gelation strategy. Int. J. Energy Res. **44**(6), 4449–4463 (2020)
15. P.-A. Le, V.-T. Nguyen, S.K. Sahoo, T.Y. Tseng, K.-H. Wei, Porous carbon materials derived from areca palm leaves for high performance symmetrical solid-state supercapacitors. J. Mater. Sci. **55**(24), 10751–10764 (2020)
16. W. Chen, X. Wang, C. Liu, M. Luo, P. Yang, X. Zhou, Rapid single-step synthesis of porous carbon from an agricultural waste for energy storage application. Waste Manag. **102**, 330–339 (2020)
17. T. Ma, X. Zhang, Y. Wang, Tassel tree flowers-derived hierarchically porous carbons with high surface area for high-performance flexible all-solid-state symmetric supercapacitors. J Energy Storage. **26**, 101014 (2019)
18. D. Yu, Y. Ma, M. Chen, X. Dong, KOH activation of wax gourd-derived carbon materials with high porosity and heteroatom content for aqueous or all-solid-state supercapacitors. J. Colloid Interface Sci. **537**, 569–578 (2018)

19. Y. Mao, N.S. Kumar, A. Dhar, A.M. Poulose, R.L. Vekariya, Economic designing of high-performance flexible supercapacitor based on cotton leaf derived porous carbon and natural ocean water. J Energy Storage. **40**(47), 102784 (2021)
20. X. Tian, H. Ma, Z. Li, S. Yan, L. Ma, F. Yu et al., Flute type micropores activated carbon from cotton stalk for high performance supercapacitors. J. Power Sources. **359**, 88–96 (2017)
21. X. Kang, C. Wang, J. Yin, Hierarchically porous carbons derived from cotton stalks for high-performance supercapacitors. ChemElectroChem **4**(10), 2599–2607 (2017)
22. X. Tian, S. Zhu, J. Peng, Y. Zuo, G. Wang, X. Guo et al., Synthesis of micro- and meso-porous carbon derived from cellulose as an electrode material for supercapacitors. Electrochim. Acta. **241**, 170–178 (2017)
23. Z. Chen, X. Peng, X. Zhang, S. Jing, L. Zhong, R. Sun, Facile synthesis of cellulose-based carbon with tunable N content for potential supercapacitor application. Carbohydr. Polym. **170**, 107–116 (2017)
24. X. Zhang, Z. Li, X. Tian, Y. Ma, L. Ma, Highly ordered micropores activated carbon from long fiber biomass for high energy density supercapacitors. ChemistrySelect **6**(45), 13015–13023 (2021)
25. X.J. Wei, Y.B. Li, S.Y. Gao, Biomass-derived interconnected carbon nanoring electrochemical capacitors with high performance in both strongly acidic and alkaline electrolytes. J. Mater. Chem. A **5**(1), 181–188 (2017)
26. C.J. Wang, D.P. Wu, H.J. Wang, Z.Y. Gao, F. Xu, K. Jiang, Nitrogen-doped two-dimensional porous carbon sheets derived from clover biomass for high performance supercapacitors. J Power Sources. **363**, 375–383 (2017)
27. S. Liu, J. Xu, J. Zhu, Y. Chang, H. Wang, Z. Liu et al., Leaf-inspired interwoven carbon nanosheet/nanotube homostructures for supercapacitors with high energy and power densities. J. Mater. Chem. A. **5**(37), 19997–20004 (2017)
28. V. Veeramani, M. Sivakumar, S.M. Chen, R. Madhu, H.R. Alamri, Z.A. Alothman et al., Lignocellulosic biomass-derived, graphene sheet-like porous activated carbon for electrochemical supercapacitor and catechin sensing. Rsc Adv. **7**(72), 45668–45675 (2017)
29. A.A. Mohammed, C. Chen, Z. Zhu, Low-cost, high-performance supercapacitor based on activated carbon electrode materials derived from baobab fruit shells. J Colloid Interface Sci. **538**, 308–319 (2019)
30. X.Y. Chen, C. Chen, Z.J. Zhang, D.H. Xie, Gelatin-derived nitrogen-doped porous carbon via a dual-template carbonization method for high performance supercapacitors. J. Mater. Chem. A **1**(36), 10903–10911 (2013)
31. S. Liu, Y. Xu, J. Wu, J. Huang, Celery-derived porous carbon materials for superior performance supercapacitors. Nanoscale Adv. **3**(18), 5363–5372 (2021)
32. N. Zhao, P. Zhang, D. Luo, W. Xiao, L. Deng, F. Qiao, Direct production of porous carbon nanosheets/particle composites from wasted litchi shell for supercapacitors. J. Alloys Compd. **788**, 677–684 (2019)
33. G. Lin, Q. Wang, X. Yang, Z. Cai, Y. Xiong, B. Huang, Preparation of phosphorus-doped porous carbon for high performance supercapacitors by one-step carbonization. RSC Adv. **10**(30), 17768–17776 (2020)
34. Y.W. Zhu, S. Murali, M.D. Stoller, K.J. Ganesh, W.W. Cai, P.J. Ferreira et al., Carbon-based supercapacitors produced by activation of graphene. Science **332**(6037), 1537–1541 (2011)
35. G. Gou, F. Huang, M. Jiang, J. Li, Z. Zhou, Hierarchical porous carbon electrode materials for supercapacitor developed from wheat straw cellulosic foam. Renew. Energ. **149**, 208–216 (2020)
36. J. Zhu, D. Xu, C. Wang, W. Qian, J. Guo, F. Yan, Ferric citrate-derived N-doped hierarchical porous carbons for oxygen reduction reaction and electrochemical supercapacitors. Carbon **115**, 1–10 (2017)
37. W. Lu, X. Cao, L. Hao, Y. Zhou, Y. Wang, Activated carbon derived from pitaya peel for supercapacitor applications with high capacitance performance. Mater. Lett. **264**, 127339 (2020)
38. F.R.M.S. Raj, N.V. Jaya, G. Boopathi, D. Kalpana, A. Pandurangan, S-doped activated mesoporous carbon derived from the *Borassus flabellifer* flower as active electrodes for supercapacitors. Mater. Chem. Phys. **240**, 122151 (2020)
39. J. Song, S. Guo, D. Ren, H. Liu, L. Kou, J. Su et al., Rice husk-derived SiOx@carbon nanocomposites as a high-performance bifunctional electrode for rechargeable batteries. Ceram. Int. **46**(8), 11570–11576 (2020)
40. S. Sankar, A.T.A. Ahmed, A.I. Inamdar, H. Im, Biomass-derived ultrathin mesoporous graphitic carbon nanoflakes as stable electrode material for high-performance supercapacitors. Mater. Des. **169**, 107688 (2019)
41. Z. Shang, X. An, H. Zhang, M. Shen, F. Baker, Y. Liu et al., Houttuynia-derived nitrogen-doped hierarchically porous carbon for high-performance supercapacitor. Carbon **161**, 62–70 (2020)
42. M. Shanmuga Priya, P. Divya, R. Rajalakshmi, A review status on characterization and electrochemical behaviour of biomass derived carbon materials for energy storage supercapacitors. Sustain. Chem. Pharm. **16**, 100243 (2020)
43. J. Wang, Z. Li, S. Yan, X. Yu, Y. Ma, L. Ma, Modifying the microstructure of algae-based active carbon and modelling supercapacitors using artificial neural networks. RSC Adv. **9**(26), 14797–14808 (2019)

44. J.C. Wang, S. Kaskel, KOH activation of carbon-based materials for energy storage. J. Mater. Chem. **22**(45), 23710–23725 (2012)
45. C. Casiraghi, A. Hartschuh, H. Qian, S. Piscanec, C. Georgi, A. Fasoli et al., Raman spectroscopy of graphene edges. Nano Lett. **9**(4), 1433–1441 (2009)
46. G.L. Sun, B. Li, J.B. Ran, X.Y. Shen, H. Tong, Three-dimensional hierarchical porous carbon/graphene composites derived from graphene oxide-chitosan hydrogels for high performance supercapacitors. Electrochim. Acta. **171**, 13–22 (2015)
47. T. Purkait, G. Singh, M. Singh, D. Kumar, R.S. Dey, Large area few-layer graphene with scalable preparation from waste biomass for high-performance supercapacitor. Sci Rep. **7**, 15239 (2017)
48. L. Yang, J. Wang, S. Wang, X. Guan, X. Guan, G. Wang, Biomass-derived multi-heteroatom-doped carbon materials for high-performance solid-state symmetric supercapacitors with superior long-term cycling stability. Ionics **26**(8), 4141–4151 (2020)
49. H.Y. Chung, G.T. Pan, Z.Y. Hong, C.T. Hsu, C.M. Huang, Biomass-derived porous carbons derived from soybean residues for high performance solid state supercapacitors. Molecules **25**(18), 4050 (2020)
50. J. Tian, T. Zhang, D. Talifu, A. Abulizi, Y. Ji, Porous carbon materials derived from waste cotton stalk with ultra-high surface area for high performance supercapacitors. Mater. Res. Bull. **143**, 111457 (2021)
51. F. Yu, Z. Ye, W. Chen, Q. Wang, H. Wang, H. Zhang et al., Plane tree bark-derived mesopore-dominant hierarchical carbon for high-voltage supercapacitors. Appl. Surf. Sci. **507**, 145190 (2020)